

Robust Late 21st Century Shift in the Regional Monsoons in RegCM-CORDEX Simulations

Moetasim Ashfaq¹, Tereza Cavazos², Michelle Simões Reboita³, José Abraham Torres-Alavez⁴, Eun-Soon Im⁵, Christiana Funmilola Olusegun⁶, Lincoln Alves⁷, Kesondra Key¹, Mojisola O. Adeniyi⁸, Moustapha Tall⁹, Mouhamadou Bamba Sylla¹⁰, Shahid Mehmood^{1,11}, Qudsia Zafar¹², Sushant Das⁴, Ismaila Diallo¹³, Erika Coppola⁴, and Filippo Giorgi⁴

¹ Computer Science and Engineering Division, Oak Ridge National Laboratory, Oak Ridge, Tennessee, USA

² Center for Scientific Research and Higher Education of Ensenada, Baja California, Mexico

³ Federal University of Itajubá, Itajubá, MG, Brazil

⁴ Abdus Salam International Centre for Theoretical Physics, Trieste, Italy

⁵ Department of Civil and Environmental Engineering/ Division of Environment and Sustainability, The Hong Kong University of Science and Technology, Hong Kong.

⁶ Centre for Atmospheric Research, National Space Research and Development Agency, Anyigba, Nigeria

⁷ National Institute for Space Research, Earth System Science Center, São José dos Campos, São Paulo, Brazil

⁸ Department of Physics, University of Ibadan, Ibadan, Nigeria

⁹ Laboratoire de Physique de l'Atmosphère et de l'Océan-Siméon Fongang, Ecole Supérieure Polytechnique, Université Cheikh Anta Diop, PO Box: 5085, Dakar-Fann, Dakar, Senegal

¹⁰ African Institute for Mathematical Sciences, AIMS Rwanda center, P. O. Box, 7150, Kigali, Rwanda

¹¹ Research Center for Environmental Changes, Taiwan International Graduate Program, Academia Sinica, Taipei, Taiwan

¹² Global Change Impact Studies Centre, Islamabad, Pakistan

¹³ Department of Geography, University of California - Los Angeles, Los Angeles, CA, USA

*Corresponding Author

Moetasim Ashfaq

Computer Science and Engineering Division

Oak Ridge National Laboratory, Oak Ridge, TN

Email: mashfaq@ornl.gov

Abstract

We use an unprecedented ensemble of regional climate model (RCM) projections over seven regional CORDEX domains to provide, for the first time, an RCM-based global view of monsoon changes at various levels of increased greenhouse gas (GHG) forcing. All regional simulations are conducted using RegCM4 at a 25km horizontal grid spacing using lateral and lower boundary forcing from three General Circulation Models (GCMs), which are part of the fifth phase of the Coupled Model Inter-comparison Project (CMIP5). Each simulation covers the period from 1970 through 2100 under two Representative Concentration Pathways (RCP2.6 and RCP8.5). Regional climate simulations exhibit high fidelity in capturing key characteristics of precipitation and atmospheric dynamics across monsoon regions in the historical period. In the future period, regional monsoons exhibit a spatially robust delay in the monsoon onset, an increase in seasonality, and a reduction in the rainy season length at higher levels of radiative forcing. All regions with substantial delays in the monsoon onset exhibit a decrease in pre-monsoon precipitation, indicating a strong connection between pre-monsoon drying and a shift in the monsoon onset. The weakening of latent heat driven atmospheric warming during the pre-monsoon period delays the overturning of atmospheric subsidence in the monsoon regions, which defers their transitioning into deep convective states. Monsoon changes under the RCP2.6 scenario are mostly within the baseline variability.

Data and Methods

Datasets:

We utilize dynamically downscaled simulations over seven CORDEX domains: Africa, Australasia, East Asia, Central America, South America, South Asia, and Southeast Asia (Figure 1). For every region, we employ ICTP RegCM4 to downscale three CMIP5 GCMs that exhibit adequate region-specific skills. Table 1 shows the details of RegCM4 domains, selected parametrizations, and driving GCMs over each region. Each RegCM4 configuration utilizes 25km horizontal grid spacing and 23 levels in the vertical over a domain that follows the latitudinal and longitudinal extent recommended by the CORDEX-CORE initiative. For GCM downscaling, RegCM4 simulations are conducted in a transient mode from 1970 to 2100 with annually varying greenhouse gas (GHG) forcing. For the historical period (1970 to 2005), RegCM4 uses observed GHG forcing. For the future period (2006 to 2100), RegCM4 is forced with projected GHG forcing RCP2.6 and RCP8.5, which represent lower and higher end radiative forcing scenarios, respectively (van Vuuren, et al. 2011). Both future period integrations are initialized using restart data from the last time step of the historical period integration.

For model comparisons with observations and reanalysis, we use i) 1° daily precipitation from the Global Precipitation Climatology Project (GPCP) version 1.2 (Huffman, et al. 2016), ii) monthly precipitation from 0.5° Climate Research Unit Timeseries (CRU TS) version 4.03 (Harris, et al. 2014), and iii) monthly atmospheric divergence, winds and temperatures from the 0.25° European Reanalysis 5 (ERA5) reanalysis data (C3S 2017).

Methods:

We utilize the *Feng et al. (2013)* analyses framework to calculate dimensionless seasonality index (hereafter seasonality), relative entropy, and the timing of centroid at each grid point. For each hydrological year (October to September), we calculate the relative entropy at each grid point using the following expression:

$$RE_y = \sum_{m=1}^{12} Pb_{y,m} \log_2 \left[\frac{Pb_{y,m}}{q_m} \right] \quad (1)$$

Where $Pb_{y,m}$ is the precipitation probability in a month m of year y , calculated as the fraction of annual precipitation in year y falling in the month m . q_m represents the uniform distribution and has value of $\frac{1}{12}$ for all months. Relative entropy provides a measure of distance between the simulated monthly precipitation and the uniform distribution. Higher values of entropy suggest the non-uniformity of monthly precipitation in a given year, implying that precipitation is more distributed around the wet season. Subsequently, seasonality of precipitation is calculated as a multiplicative product of relative entropy and the annual mean precipitation. In order for the results to be comparable across different CORDEX domains, datasets (observations, model simulations), and simulation periods (historical, future), we normalize the results using the maximum precipitation (P_{max}) found over all datasets and simulation periods. Therefore, the expression for seasonality can be written as:

$$S_y = RE \times \frac{P_y}{P_{max}} \quad (2)$$

The maximum value of seasonality can be reached if a grid point receives P_{max} in a single month, which implies that regions with low annual precipitation will exhibit low seasonality even if precipitation distribution across the months is highly nonuniform.

Furthermore, we calculate the timing of centroid using the first moments of monthly mean precipitation, which corresponds to the timing when 50% of the annual precipitation is reached in a hydrological year. Further details of the methodology and mathematical expressions can be referred to *Feng et al. (2013)*.

Additionally, we calculate the monsoon onset pentad (5-day average) at each grid point following a methodology adopted from *Bombardi and Carvalho (2009)*. For each analysis time period, we use the climatological pentad time series at each grid point to calculate the sum using the following expression:

$$S(\text{pentad}) = \sum_{n=\text{pentad}_1}^{\text{pentad}} (P_n - \bar{P}) \quad (3)$$

Where \bar{P} represents the climatological annual mean and P_n represents the n th pentad of precipitation. Subsequently, the monsoon onset and monsoon demise at each grid point are defined as the pentad after the minimum S and the pentad after the maximum S, respectively. Our approach is relatively simple and slightly different when compared to *Bombardi and Carvalho (2009)*, yet it yields similar results when applied to the climatological data.

We utilize 1995 to 2014 as the reference historical period used for comparisons with observations and reanalysis, and for the calculation of future changes in the 21st century. The reference period during 2006 to 2014 is taken from the RCP8.5 simulations. There is not much difference between RCP8.5 and RCP2.6 radiative forcing, and corresponding RegCM4 simulations for this time period. Therefore, no noticeable impact on future changes are expected due to this methodological choice. We use two 20-year time slices from the RCP2.6 and RCP8.5 model integrations to calculate changes in the mid-century (2041 to 2060) and the late century (2080 to 2099) period. All results are shown as an ensemble mean of three ensemble members

over each domain while the robustness of future changes is being tested using the baseline variability as a threshold at each grid point. The late century period (2080 to 2099) changes over Africa are based on the downscaling of only two GCMs (HadGEM2-ES and NorESM1-M, Table 1), since the third ensemble member was not available at the time of analyses.

Summary of Results:

In this study, we have provided, for the first time, a global view of changes in monsoon characteristics based on a large ensemble of high-resolution RegCM4 experiments for two different GHG forcing scenarios. The evaluations of the RegCM4 ensemble mean demonstrates the ability of the model to reasonably reproduce the inter-hemispheric transition of the monsoon seasons and the evolution of the seasonal monsoon characteristics in different regions. Monsoon systems around the world are projected to experience unprecedented changes in monsoon precipitation characteristics, including shrinking of the rainy season, delays in monsoon onset and demise, and substantial changes in the magnitude of seasonal precipitation, especially under the high-end RCP8.5 scenario. For this scenario, most of the projected changes become spatially robust and greater than the baseline variability towards the end of the 21st century. A robust relationship between the projected pre-monsoon drying and delays in the monsoon onset exists across regional monsoons, as a weakening of latent heat driven atmospheric warming during the pre-monsoon period delays the overturning of atmospheric subsidence in the monsoon regions. In response to the RCP2.6 forcing, which corresponds to a scenario of strongly reduced GHG emissions by the end of the century, most of the regional monsoons exhibit small changes within the baseline variability. This illustrates the strong added value in reducing emissions for global economies, in particular, for currently poor and more vulnerable tropical countries.

Acknowledgements:

Support for model simulations, data storage and analyses are partly provided by the Oak Ridge Leadership Computing Facility at the Oak Ridge National Laboratory (ORNL). M. A. was supported by the National Climate-Computing Research Center, which is located within the National Center for Computational Sciences at the ORNL and supported under a Strategic Partnership Project, 2316-T849-08, between DOE and NOAA. M.S.R would like to thank CNPq-Brazil. E.S.M was supported by the Hong Kong Research Grants Council funded project, GRF16309719.

Region	Physics Schemes	Parameterization	Driving GCMs
Africa 500x480 (25km)	Boundary Layer	Holtslag [1]	HadGEM2-ES [2] MPI-ESM-MR [3] NorESM1-M [4]
	Cumulus (Land)	Tiedtke [5]	
	Cumulus (Ocean)	Kain-Fritsch [6, 7]	
	Microphysics	SUBEX [8]	
	Ocean Flux	Zeng [9]	
Australasia 338x416 (25km)	Boundary Layer	Holtslag	HadGEM2-ES MPI-ESM-MR NorESM1-M
	Cumulus (Land)	Tiedtke	
	Cumulus (Ocean)	Tiedtke	
	Microphysics	SUBEX	
	Ocean Flux	Zeng	
Central America 573x373 (25km)	Boundary Layer	Holtslag	HadGEM2-ES MPI-ESM-MR GFDL-ESM2M [10]
	Cumulus (Land)	Emanuel [11]	
	Cumulus (Ocean)	Kain-Fritsch	
	Microphysics	SUBEX	
	Ocean Flux	Zeng et al.	
South America 363x333 (25km)	Boundary Layer	Holtslag	HadGEM2-ES MPI-ESM-MR NorESM1-M
	Cumulus (Land)	Tiedtke	
	Cumulus (Ocean)	Kain-Fritsch	
	Microphysics	SUBEX	
	Ocean Flux	Zeng	
South Asia 429x337 (25km)	Boundary Layer	UW PBL [12]	HadGEM2-ES MPI-ESM-MR MIROC5 [13]
	Cumulus (Land)	Emanuel	
	Cumulus (Ocean)	Tiedtke	
	Microphysics	SUBEX	
	Ocean Flux	Zeng et al.	
Southeast Asia 338x192 (25km)	Boundary Layer	Holtslag	HadGEM2-ES MPI-ESM-MR NorESM1-M
	Cumulus (Land)	Tiedtke	
	Cumulus (Ocean)	Tiedtke	
	Microphysics	SUBEX	
	Ocean Flux	Zeng	
East Asia 384x250 (25km)	Boundary Layer	Holtslag	HadGEM2-ES MPI-ESM-MR NorESM1-M
	Cumulus (Land)	Emanuel	
	Cumulus (Ocean)	Emanuel	
	Microphysics	SUBEX	
	Ocean Flux	Zeng	

Table 1 RegCM4 configuration over various CORDEX domains

- Holtslag, A.A.M., E.I.F. Debruijn, and H.L. Pan, *A High-Resolution Air-Mass Transformation Model for Short-Range Weather Forecasting*. Monthly Weather Review, 1990. **118**(8): p. 1561-1575.
- Jones, C.D., et al., *The HadGEM2-ES implementation of CMIP5 centennial simulations*. Geoscientific Model Development, 2011. **4**(3): p. 543-570.
- Stevens, B., et al., *Atmospheric component of the MPI-M Earth System Model: ECHAM6*. Journal of Advances in Modeling Earth Systems, 2013. **5**(2): p. 146-172.
- Bentsen, M., et al., *The Norwegian Earth System Model, NorESM1-M - Part 1: Description and basic evaluation of the physical climate*. Geoscientific Model Development, 2013. **6**(3): p. 687-720.
- Tiedtke, M., *An extension of cloud-radiation parameterization in the ECMWF model: The representation of subgrid-scale variations of optical depth*. Monthly Weather Review, 1996. **124**(4): p. 745-750.
- Kain, J.S. and J.M. Fritsch, *A One-Dimensional Entraining Detraining Plume Model and Its Application in Convective Parameterization*. Journal of the Atmospheric Sciences, 1990. **47**(23): p. 2784-2802.
- Kain, J.S., *The Kain-Fritsch convective parameterization: An update*. Journal of Applied Meteorology, 2004. **43**(1): p. 170-181.
- Pal, J.S., E.E. Small, and E.A.B. Eltahir, *Simulation of regional-scale water and energy budgets: Representation of subgrid cloud and precipitation processes within RegCM*. Journal of Geophysical Research-Atmospheres, 2000. **105**(D24): p. 29579-29594.
- Zeng, X.B., M. Zhao, and R.E. Dickinson, *Intercomparison of bulk aerodynamic algorithms for the computation of sea surface fluxes using TOGA COARE and TAO data*. Journal of Climate, 1998. **11**(10): p. 2628-2644.
- Donner, L.J., et al., *The Dynamical Core, Physical Parameterizations, and Basic Simulation Characteristics of the Atmospheric Component AM3 of the GFDL Global Coupled Model CM3*. Journal of Climate, 2011. **24**(13): p. 3484-3519.
- Emanuel, K.A., *A Scheme for Representing Cumulus Convection in Large-Scale Models*. Journal of the Atmospheric Sciences, 1991. **48**(21): p. 2313-2335.
- Bretherton, C.S., J.R. McCaa, and H. Grenier, *A new parameterization for shallow cumulus convection and its application to marine subtropical cloud-topped boundary layers. Part I: Description and 1D results*. Monthly Weather Review, 2004. **132**(4): p. 864-882.
- Watanabe, M., et al., *Improved Climate Simulation by MIROC5. Mean States, Variability, and Climate Sensitivity*. Journal of Climate, 2010. **23**(23): p. 6312-6335.

RegCM CORDEX Domains and Monsoon Regions

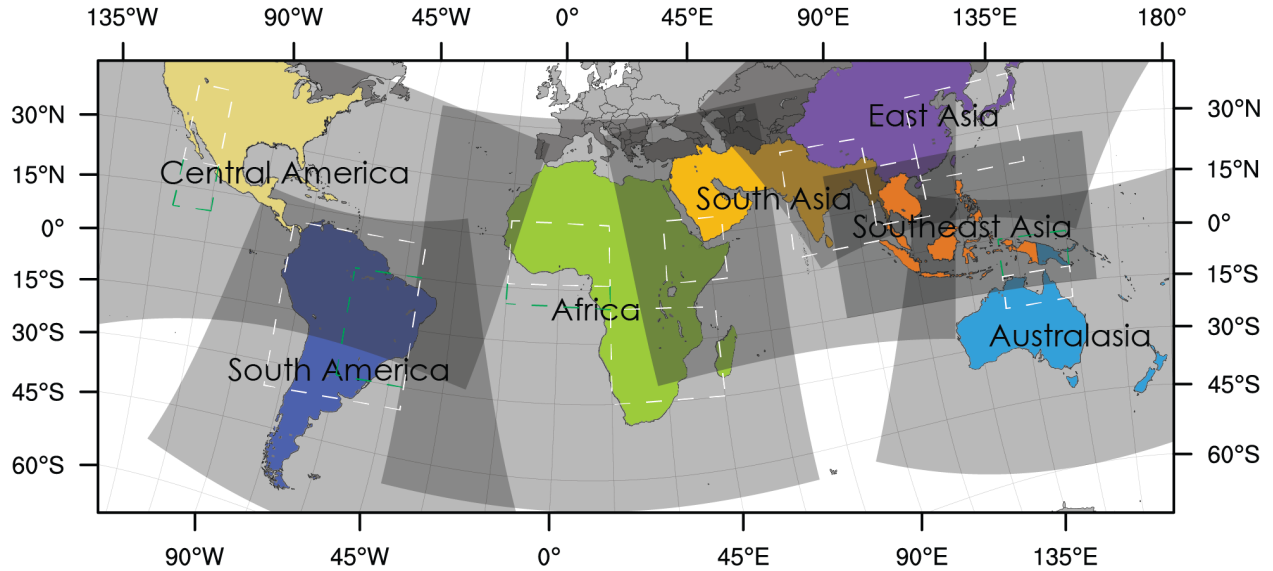


Figure 1. Different RegCM CORDEX domains used in the analyses. The colored land area within each domain reflects the region that has been used from each RegCM integration for spatial plots. Boxes represent areas used for various zonal average analyses.

Precipitation Characteristics over Monsoon Regions

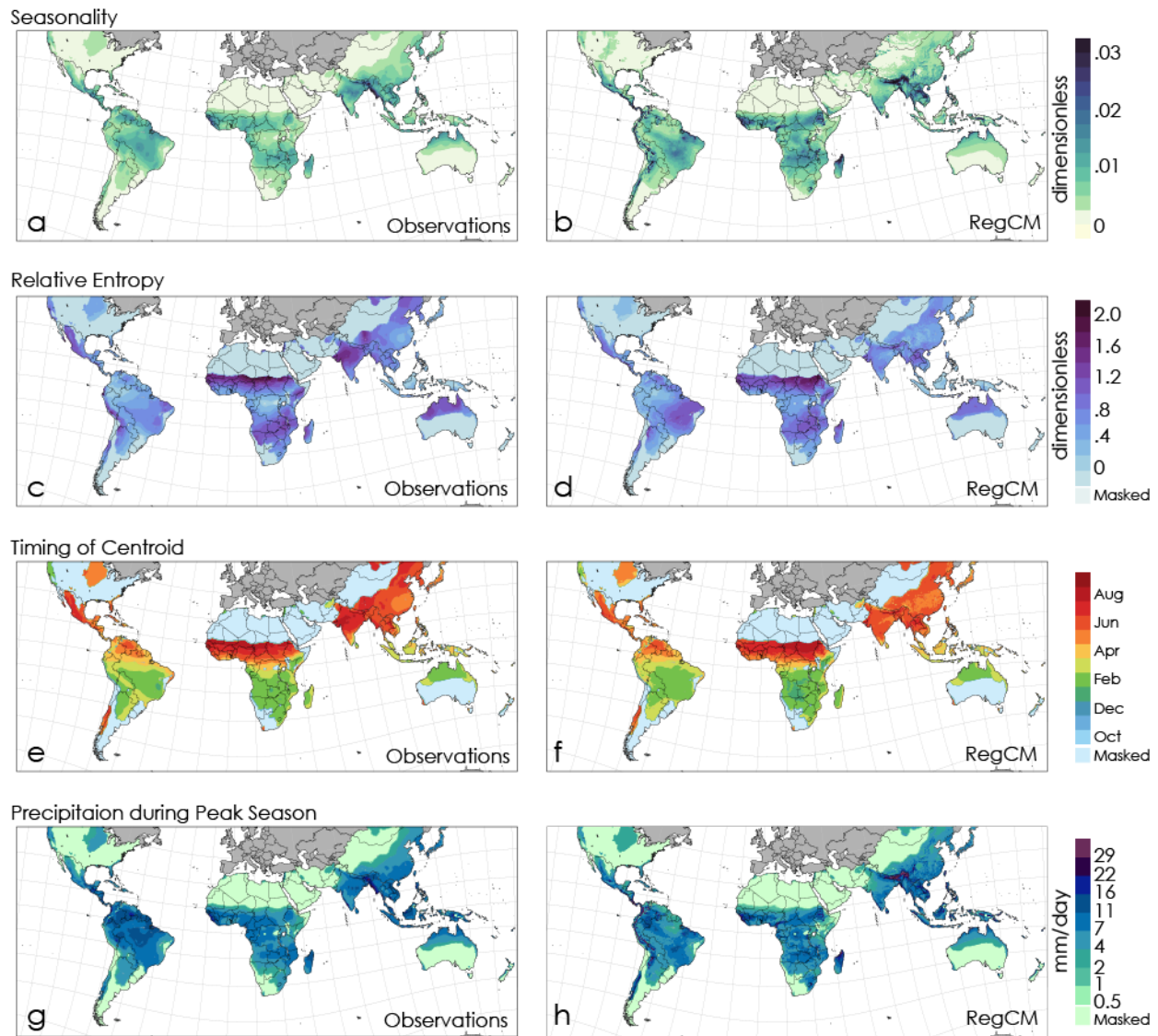


Figure 2. Comparison between the CRU observations and the RegCM ensemble mean during the 1995 to 2014 period. Seasonality (a, b), relative entropy (c, d), timing of centroid (e, f), peak season precipitation (g, h). Values are masked in the bottom three rows where seasonality is < 0.025.

Monsoon Onset and Demise 1995 to 2014)

Monsoon Onset

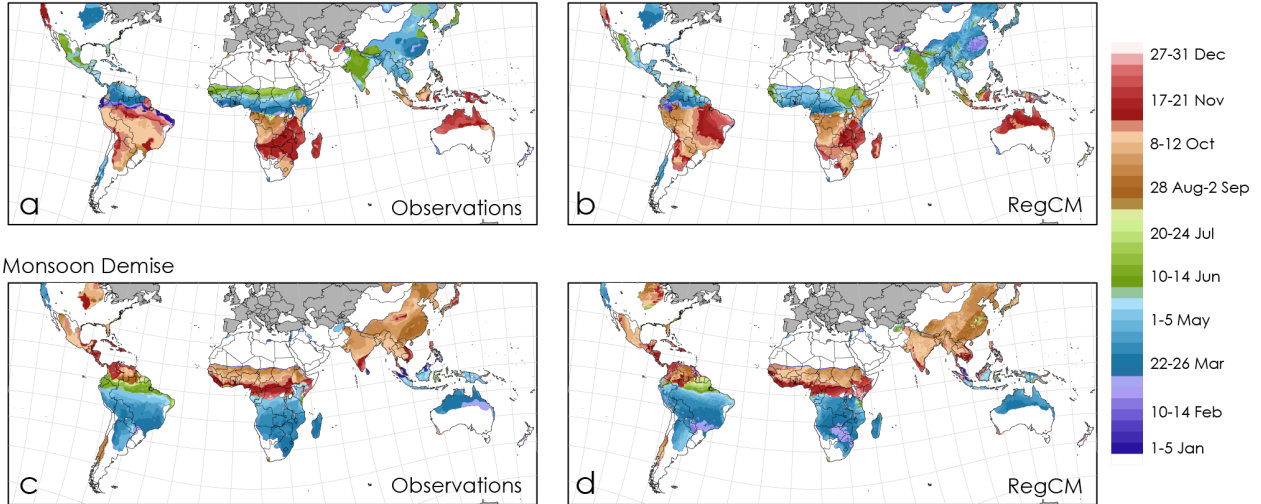


Figure 3. Monsoon onset and demise over land in the reference period (1995 to 2014) in the GPCP Observations (a,c), and the RegCM ensemble (b,d). White land areas are masked where observed seasonality is < 0.025 . Results are not meaningful outside the monsoon regions.

Near-term Future (2041 to 2060) Changes w.r.t. 1995 to 2014

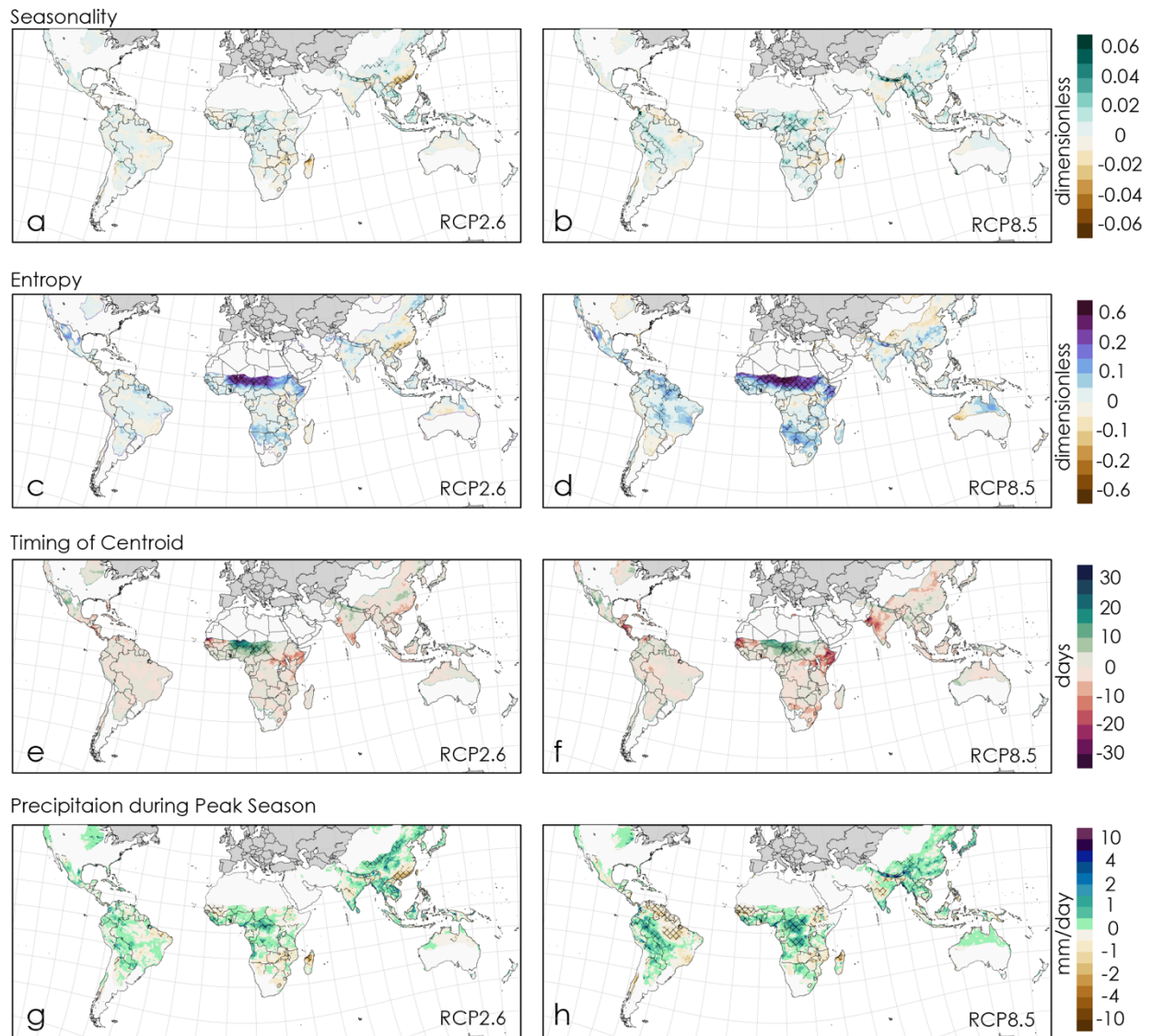


Figure 4. Simulated projected changes in the near-term future (2041 to 2060) with respect to the 1995 to 2014 period under RCP2.6 and RCP8.5. Seasonality (a, b), entropy (c, d), timing of centroid (e, f), peak season precipitation (g, h). Stippling represents those regions where projected changes are greater than the reference period variability. White land areas are masked where observed seasonality is < 0.025 .

Long-term Future (2080 to 2099) Changes w.r.t. 1995 to 2014

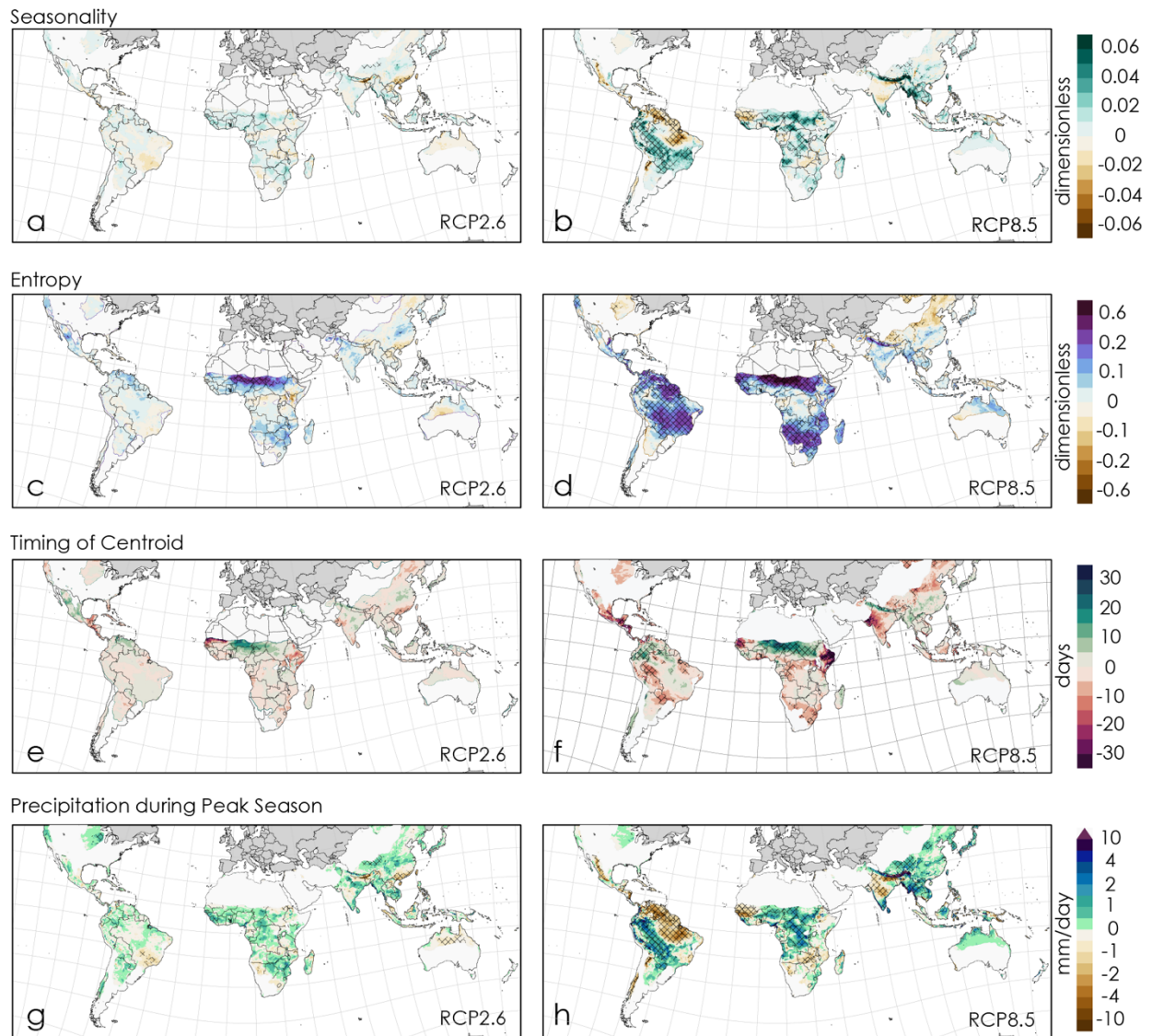


Figure 5. Simulated projected changes in the far future (2080 to 2099) with respect to the 1995 to 2014 period under RCP2.6 and RCP8.5. Seasonality (a, b), entropy (c, d), timing of centroid (e, f), peak season precipitation (g, h). Stippling represents those regions where projected changes are greater than the reference period variability. White land areas are masked where observed seasonality is < 0.025 .

Future Changes w.r.t. 1995 to 2014

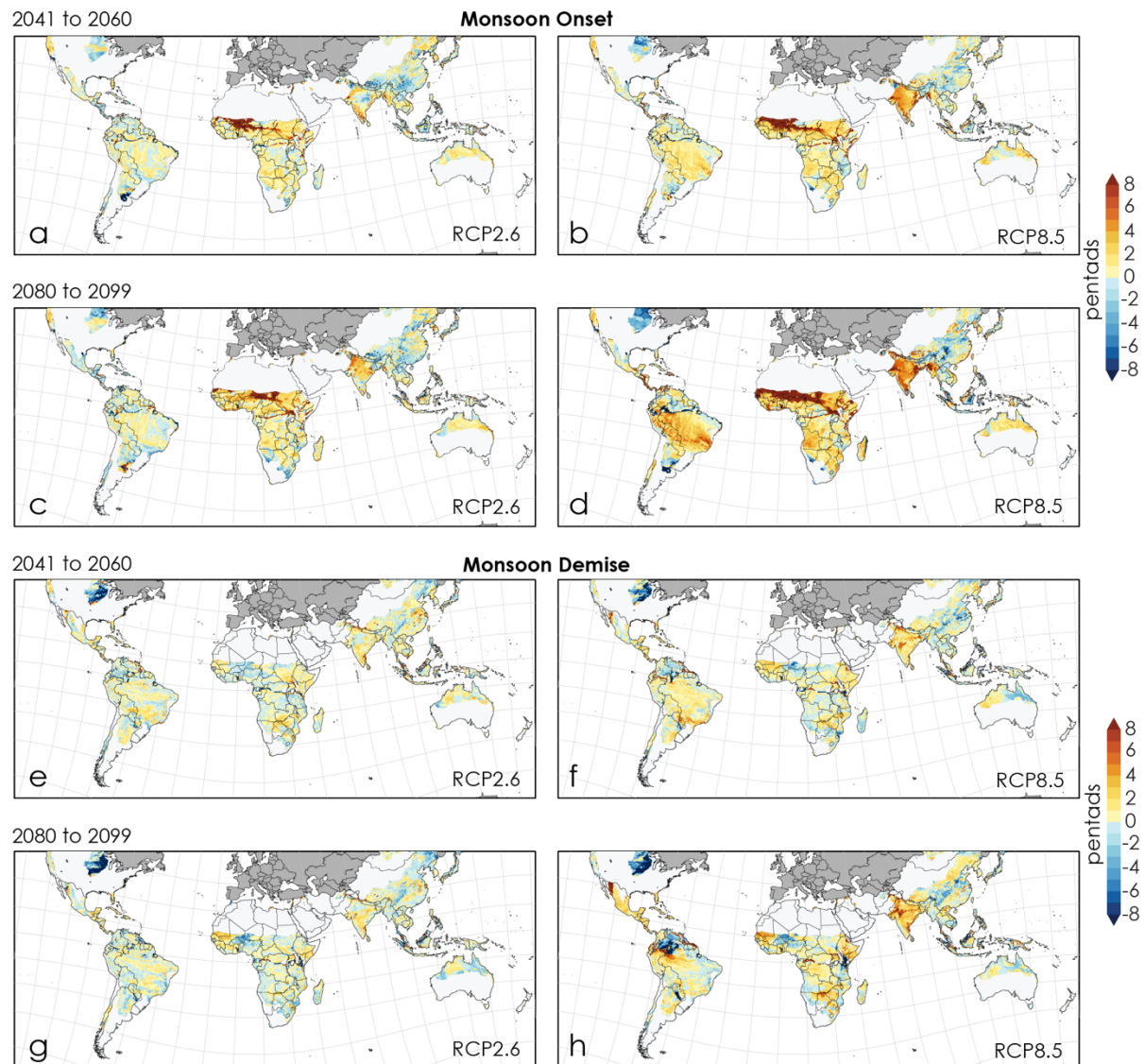


Figure 6. Simulated projected changes in the monsoon onset (a to d) and demise (e to h) in the RCP2.6 (left column) and the RCP8.5 (right column). Changes are shown for the near-term (2041 to 2060) and the long-term (2080 to 2099) with respect to 1995 to 2014. White land areas are masked where observed seasonality is < 0.025 . Results are not meaningful outside the monsoon regions.

Divergence ($\times 10^6$) and Vertical Velocity ($\times 50$) Vectors with Vertical Velocity ($\times 50$) as Colored Contours

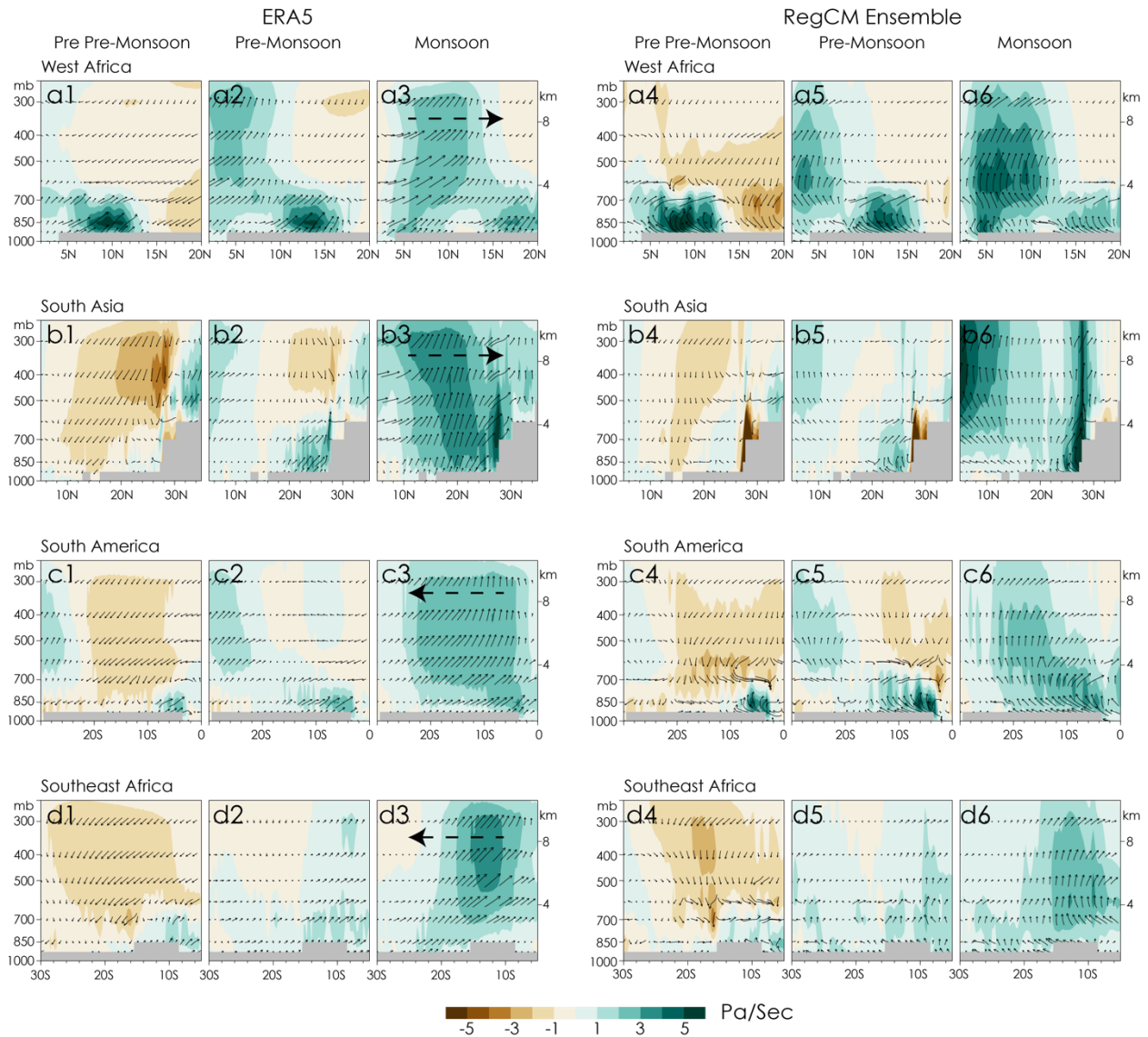


Figure 7. Latitude-height cross-section of divergence ($1/s$) and vertical pressure velocity (Pa/s) in ERA5 (left three columns) and RegCM (right three columns), shown as wind vectors averaged over West Africa (a1-a6; 15W to 15E, 2N to 20N), South Asia (b1-b6; 70E to 95E, 5N to 35N), South America (c1-c6; 60W to 40W, 0 to 30S), and Southeast Africa (d1-d6; 15E to 45E, 5S to 30S). Colored contours represent vertical pressure velocity. Black arrows represent the direction of the monsoon along the latitude. Both vertical pressure velocity and divergence have been exaggerated by 50 and 10^6 in all plots. Vertical pressure velocity is multiplied by -1 so that positive values represent an upward motion. The three panels in each case represent averages over pre pre-monsoon, pre-monsoon and monsoon periods. The Pre-monsoon period represents the average over the two months prior to the monsoon season. The pre pre-monsoon period represents the average over

Divergence ($\times 10^6$) and Vertical Velocity ($\times 50$) Vectors with Vertical Velocity ($\times 50$) as Colored Contours

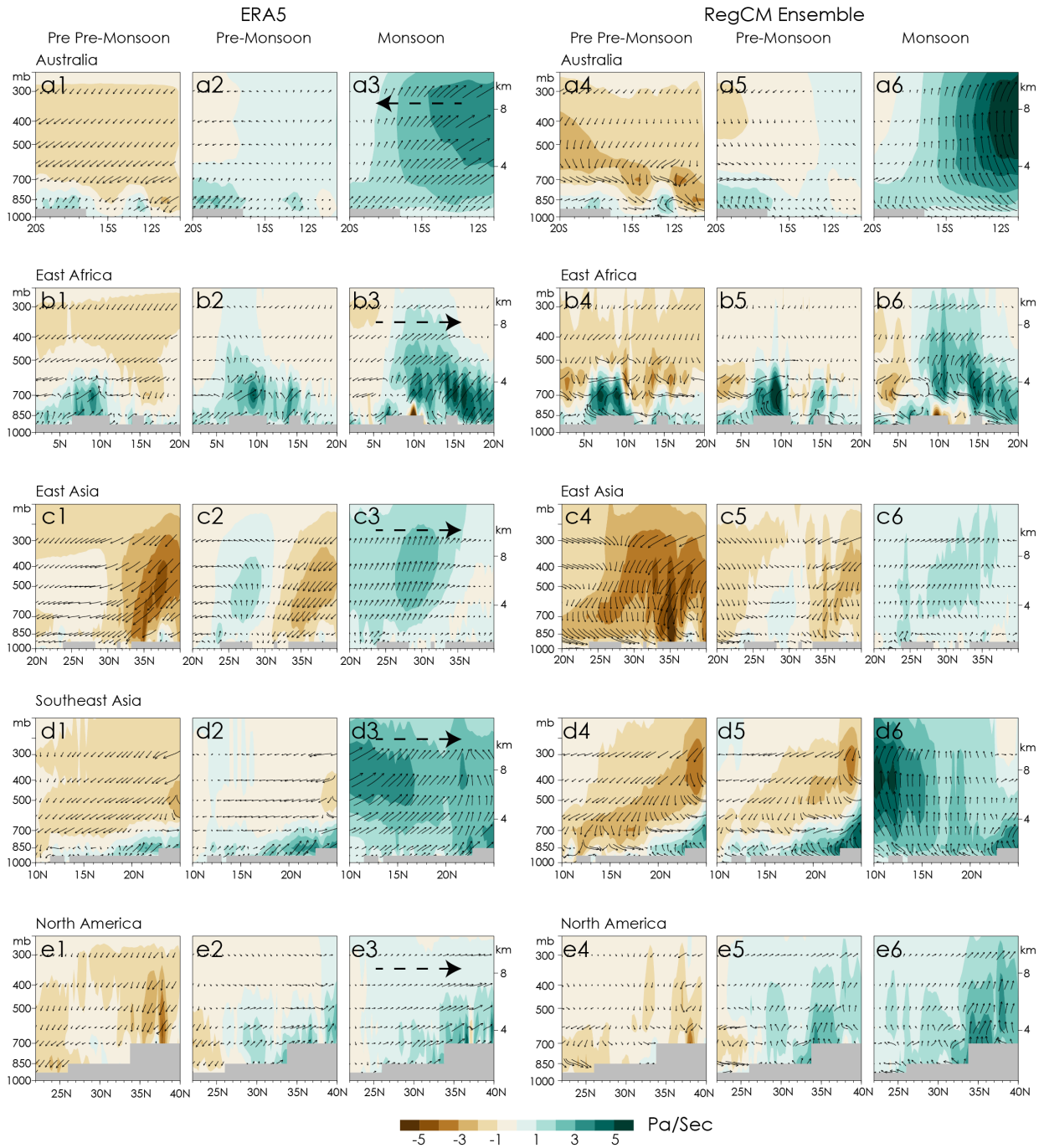


Figure 8. Same as in Figure 7 but over Australia (a1-a6; 130E to 150E, 10S to 20S), East Africa (b1-b6; 32E to 50E, 2N to 20N), East Asia (c1-c6; 110E to 140E, 20N to 40N), Southeast Asia (d1-d6; 95E to 110E, 10N to 25N), and North America (e1-e6; 114W to 104W, 22N to 40N).

Zonally Averaged Precipitation over Monsoon Regions

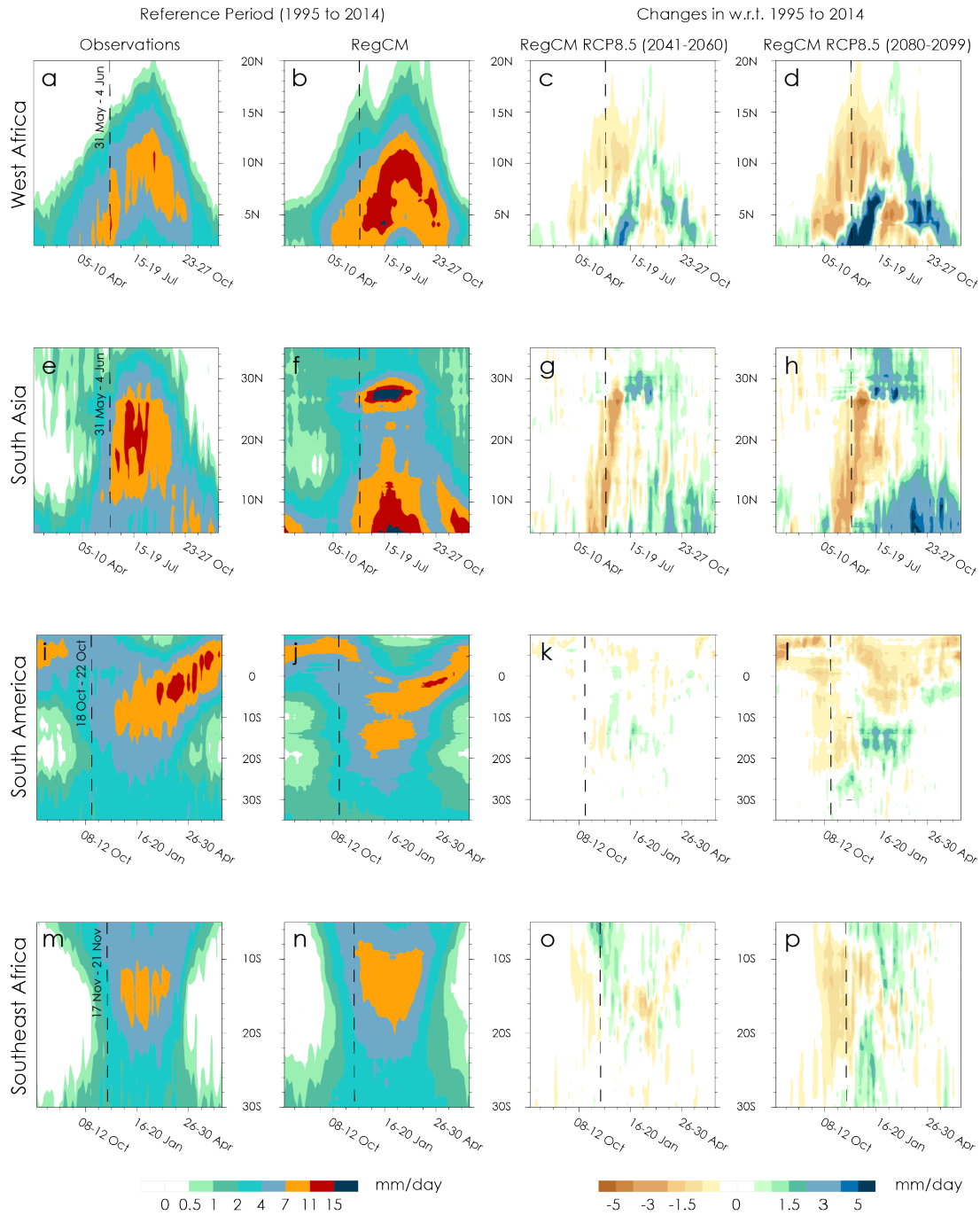


Figure 9. Zonally averaged 5-day mean precipitation (1995 to 2014) in the GPCP observations (first column) and in the RegCM simulations (second column) over West Africa (a, b; 15W to 15E, 2N to 20N), South Asia (e, f; 70E to 95E, 5N to 35N), South America (i, j; 80W to 40W, 10N to 35S), and Southeast Africa (m, n; 15E to 45E, 5S to 30S). Mid-term (2041 to 2060) and long-term (2080 to 2099) future changes in zonal average 5-day mean precipitation under RCP8.5. Africa (c, d), South Asia (g, h), South America (k, l), and South Africa (o, p). The vertical lines in each panel represent the approximate climatological timing (in pentads) by when most of the region receives earliest monsoon precipitation in the observations as shown in Figure 3.

Zonally Averaged Precipitation over Monsoon Regions

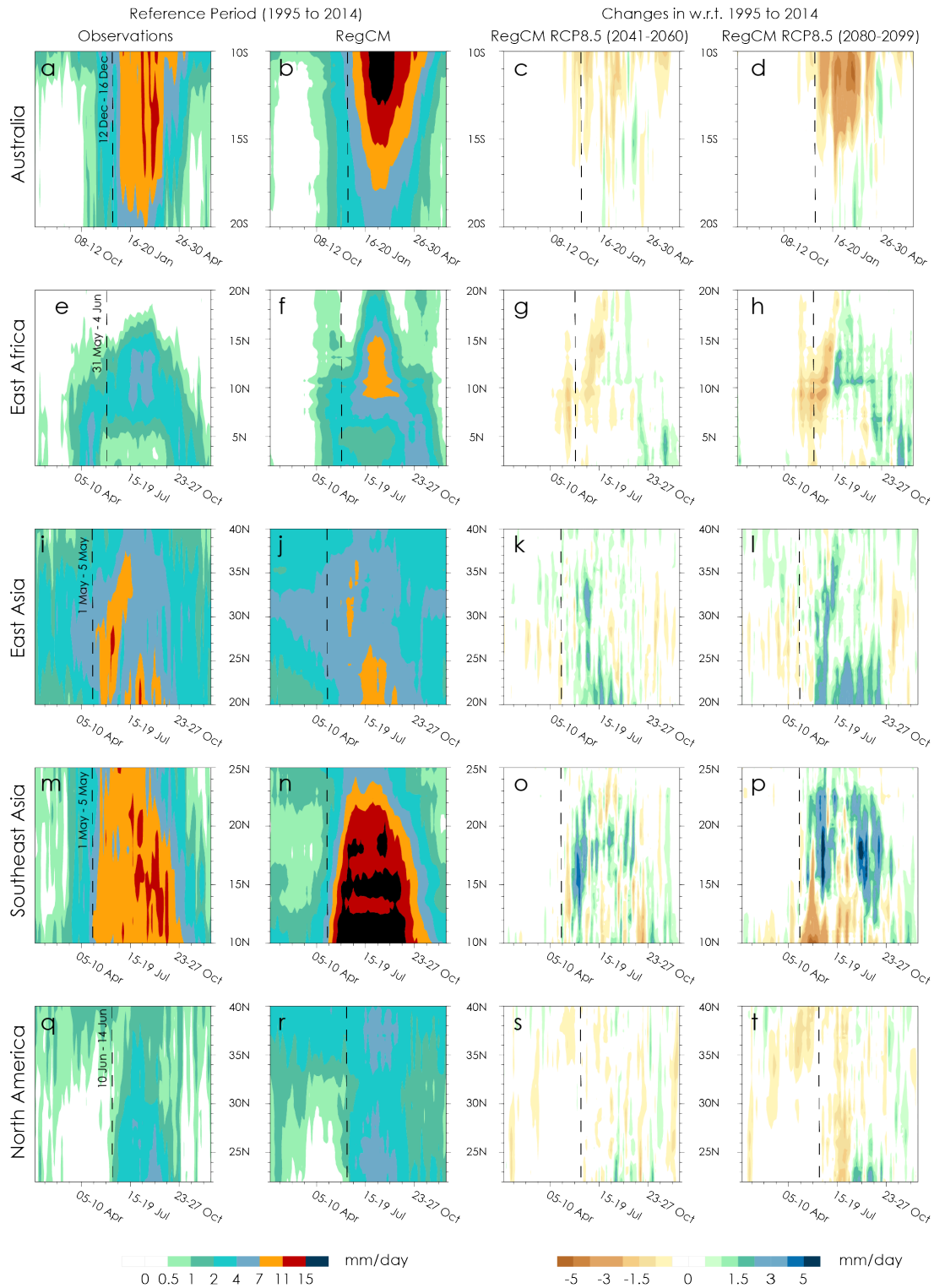
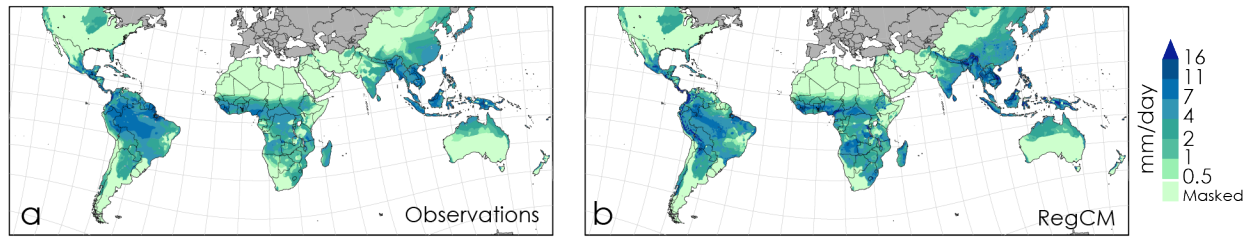


Figure 10. Same as in Figure 9 but for Australia (a-d; 130E to 150E, 10S to 20S), East Africa (e-h; 32E to 50E, 2N to 20N), East Asia (i-l; 110E to 140E, 20N to 40N), Southeast Asia (m-p; 95E to 110E, 10N to 25N), and North America (q-t; 114W to 104W, 22N to 40N).

Average Pre-monsoon Precipitation (1995 to 2014)



Changes in Average Pre-monsoon Precipitation w.r.t 1995 to 2014

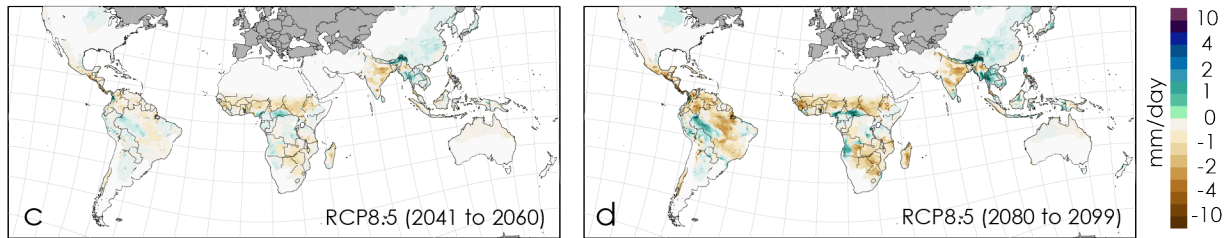


Figure 11. Pre-monsoon precipitation during 1995 to 2014 in a) CRU observations, b) RegCM ensemble. Changes w.r.t. 1995 to 2014 in pre-monsoon precipitation during c) 2041 to 2060 and d) 2080 to 2099 under RCP8.5. The pre-monsoon precipitation represents the average of the two months before the monsoon season.

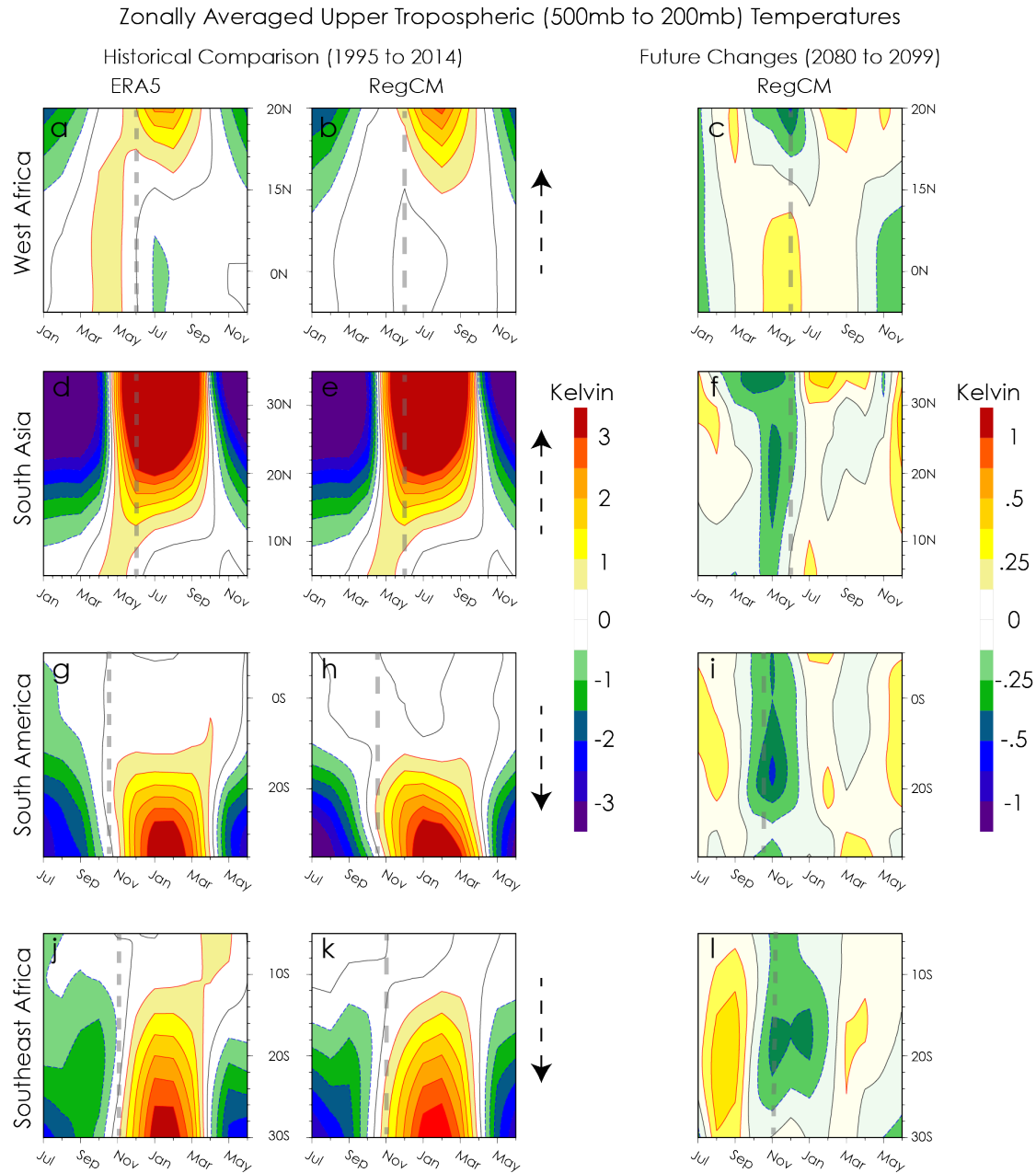


Figure 12. Departure of zonally averaged monthly upper tropospheric temperatures from the annual mean over West Africa (a to c), South Asia (d to f), South America (g to i) and Southeast Africa (j to l). The first and second column show comparisons between ERA5 and RegCM in the reference period (1995 to 2014). The third column shows the projected changes in the late-century (2080 to 2099) period under RCP8.5 with respect to the reference period. All domains are identical to the ones used in Figure 7, except for West Africa, which extends further down to 5S. Black contours represent the zero line. The grey dotted line represents approximate timing of the earliest onset over land and the black arrows represent the direction of the monsoon progression along the latitude over each region.

Zonally Averaged Upper Tropospheric (500mb to 200mb) Temperatures

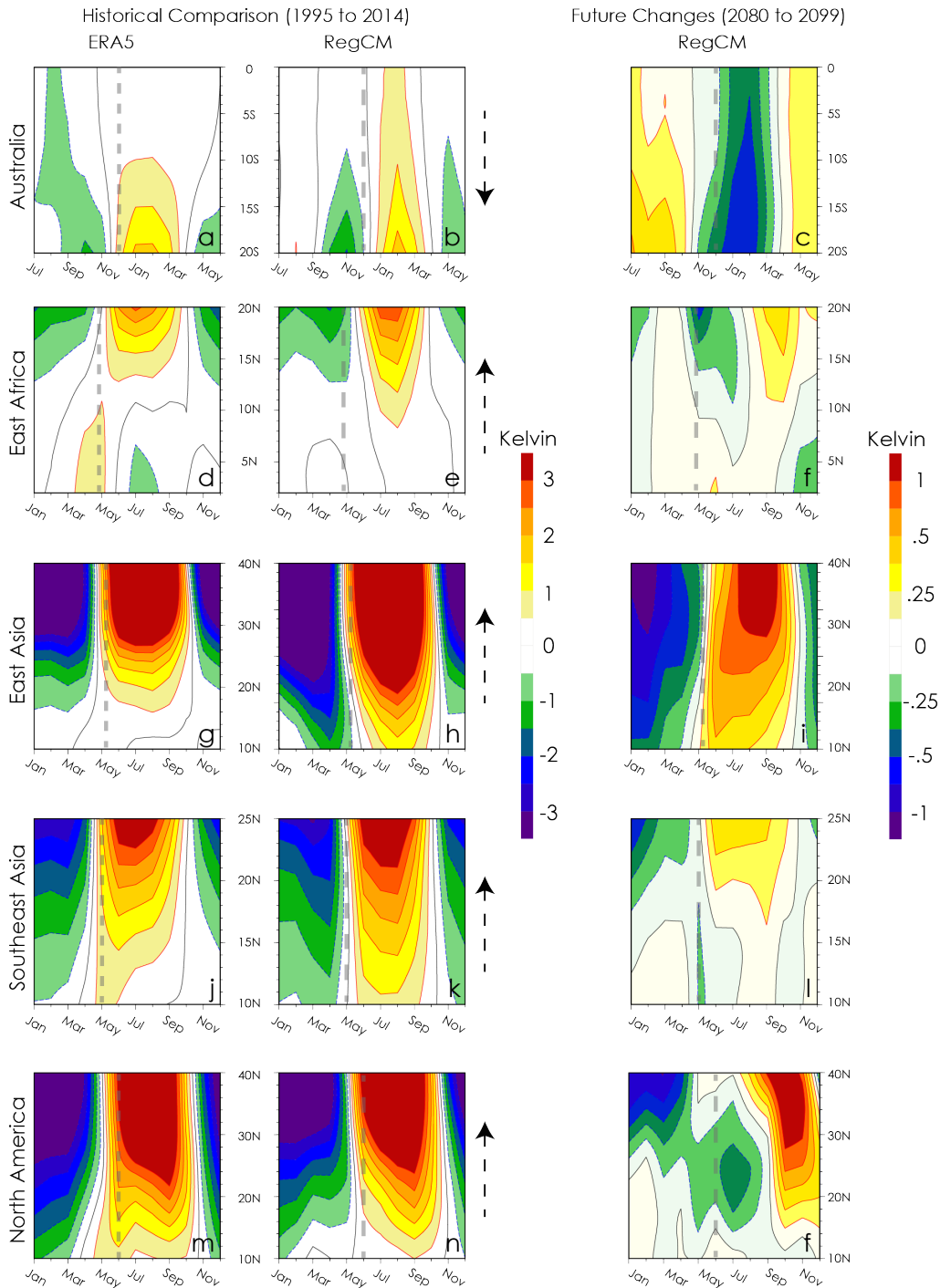


Figure 13. Same as in Figure 12, but for Australia (a to c), East Africa (d to f), East Asia (g to i), Southeast Asia (j to l) and North America (m to o). All domains are identical to the ones used in Figure 7, except for Australia, which extends further north to the equator, and North America, which extends further down to 10N. The black contours represent the zero line. The grey dotted line represents the approximate timing of the earliest onset over land and the black arrows represent the direction of the monsoon progression along the latitude over each region.

Divergence ($\times 10^6$) and Vertical Velocity ($\times 50$) Vectors with Vertical Velocity ($\times 50$)
as Colored Contours (Changes in RCP8.5 2080 to 2099 w.r.t 1995 to 2014)

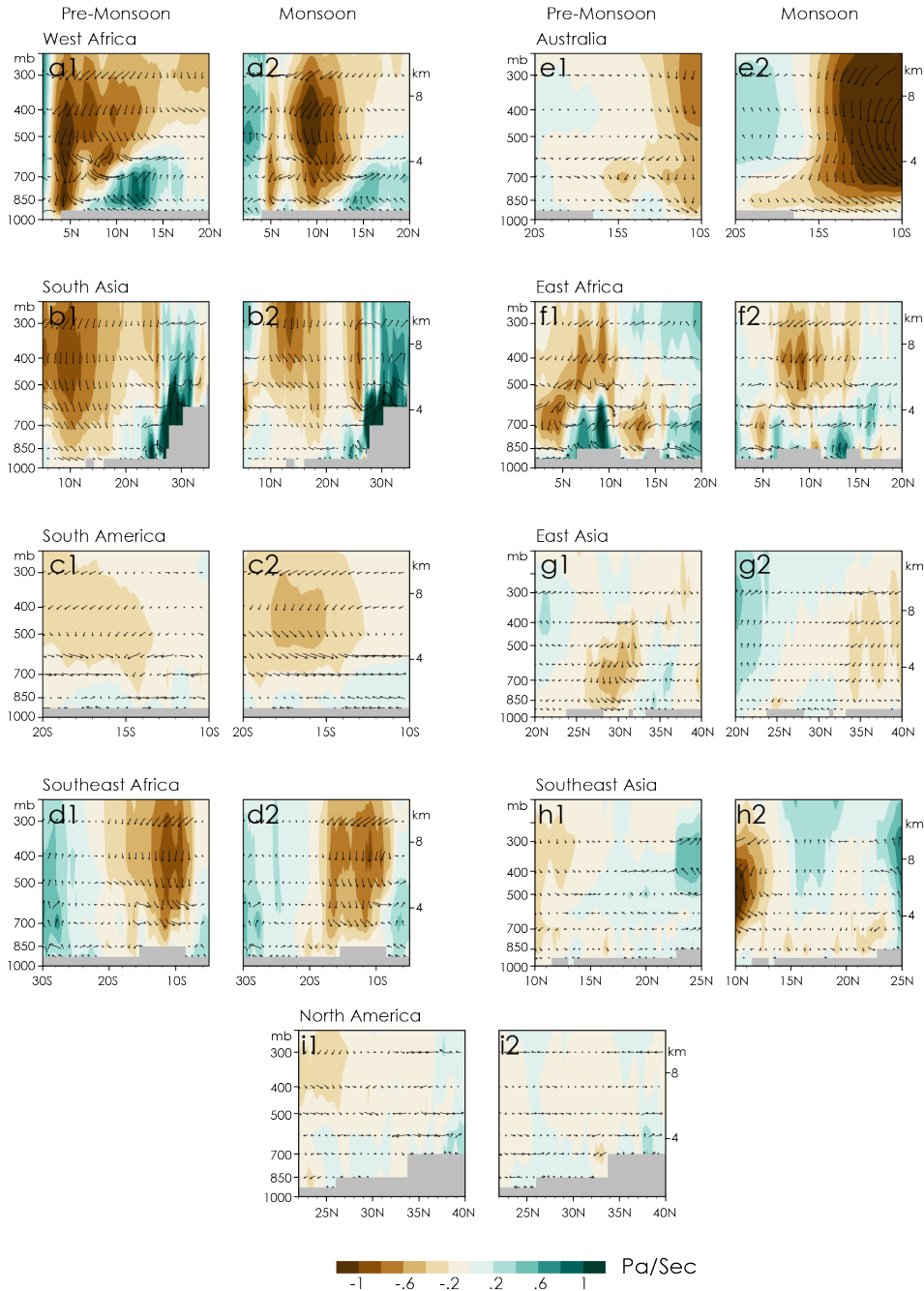


Figure 14. Changes (RCP8.5 2080 to 2099 w.r.t 1995 to 2014) in latitude-height cross-section of divergence ($1/s$) and vertical pressure velocity (Pa/s), shown as wind vectors averaged over latitudes used in Figure 7 and 8. West Africa (a1, a2), South Asia (b1, b2), South America (c1, c2), and Southeast Africa (d1, d2), Australia (e1, e2), East Africa (f1, f2), East Asia (g1, g2), Southeast Asia (h1, h2) and North America (i1, i2). Colored contours represent the vertical pressure velocity. Both vertical pressure velocity and divergence have been exaggerated by 50 and 10^6 in all plots. Vertical pressure velocity is multiplied by -1 so that positive values represent an upward motion. The two panels in each case represent the averages over the pre-monsoon and monsoon periods. The pre-monsoon period represents the average over two months prior to the monsoon season.